Heliyon 10 (2024) e23588

Contents lists available at ScienceDirect

Heliyon

journal homepage: www.cell.com/heliyon

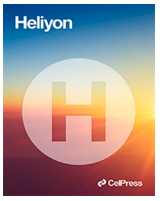

Effect of non-uniform heat rise/fall and porosity on MHD Williamson hybrid nanofluid flow over incessantly moving thin needle

Amir Abbas [a,*], Abid Hussanan [b], Adebowale Martins Obalalu [c], Karim Kriaa [d], Chemseddine Maatki [e], Bilel Hadrich [d], Muhammad Aslam [f], Lioua Kolsi [g,h]

[a] Department of Mathematics, Faculty of Science, University of Gujrat, Sub-Campus Mandi Bahauddin, Mandi Bahauddin, 50400, Pakistan
[b] Department of Mathematics, Division of Science and Technology, University of Education, Lahore, 54000, Pakistan
[c] Department of Mathematical Sciences, Augustine University Ilara-Epe, Lagos, Nigeria
[d] Department of Chemical Engineering, College of Engineering, Imam Mohammad Ibn Saud Islamic University (IMSIU), Riyadh, 11432, Saudi Arabia
[e] Department of Mechanical Engineering, College of Engineering, Imam Mohammad Ibn Saud Islamic University (IMSIU), Riyadh, 11432, Saudi Arabia
[f] Institute of Physics and Technology, Ural Federal University, Mira Str.19, 620002, Yekaterinburg, Russia
[g] Department of Mechanical Engineering, College of Engineering, University of Ha'il, Ha'il City, 81451, Saudi Arabia
[h] Laboratory of Metrology and Energy Systems, Department of Energy Engineering, University of Monastir, Monastir, 5000, Tunisia

ARTICLE INFO

Keywords:
Hybrid nanofluid
Porous medium
Magnetohydrodynamics
Williamson fluid
Thin needle
Non-uniform heat rise/fall

ABSTRACT

In this work, a novel enhanced model of the thermophysical characteristics of hybrid nanofluid is introduced. An innovative kind of fluid called hybrid nanofluid has been engineered to increase the heat transfer rate of heat and performance of thermal system. A growing trend in scientific and industrial applications pushed researchers to establish mathematical models for non-Newtonian fluids. A parametric study on theheat transfer and fluid flow of a Williamson hybrid nanofluid based on AA7075-AA7072/Methanol overincessantly moving thin needle under the porosity, Lorentz force, and non-uniform heat rise/fallis performed. Due to similarity variables, the partial differential equations governing the studied configuration undergo appropriate transformation to be converted into ordinary differential equations. The rigorous built-in numerical solver in bvp4c MATLAB has been employed to determine the numerical solutions of the established non-linear ordinary differential equations. It is worthy to note that velocity declines for both AA7075/Methanol nanofluid and AA7075- AA7072/Methanol hybrid nanofluid, but highervelocitymagnitudes occur for theAA7075/Methanol whilethe Williamson fluid parameters increased. It is alsoconcluded that as the porosity parameter isincreased, the flow intensity decreases gradually. It is worthy to note that for both non-uniform heat-rise and fall parameters, the temperature of the fluid gets stronger. Mounting valuesof needle thickness parameter leads to reduction in fluid speed and temperature. It is noticedthat as volume fractions of both types of nanoparticles are augmented then fluidvelocity and temperature amplify rapidly. A Comparison of current and published results is performed to ensure the validity of the established numerical model.

* Corresponding author.
E-mail addresses: cfdamirabbas4693@gmail.com (A. Abbas), abid.hussanan@ue.edu.pk (A. Hussanan), adebowale.obalalu17@gmail.com (A.M. Obalalu), kskriaa@imamu.edu.sa (K. Kriaa), casmaatki@imamu.edu.sa (C. Maatki), bmhadrich@imamu.edu.sa (B. Hadrich), lioua_enim@yahoo.fr (L. Kolsi).

https://doi.org/10.1016/j.heliyon.2023.e23588
Received 31 July 2023; Received in revised form 25 November 2023; Accepted 7 December 2023
Available online 12 December 2023

Nomenclature

μ_{hnf}	Dynamic viscosity of hybrid nanofluid: Unit $(Pa.s)$, Dimension $[ML^{-1}T^{-1}]$
NF	Nanofluid
HNF	Hybrid nanofluid
μ_f	Dynamic viscosity of base fluid: Unit $(Pa.s)$,Dimension $[ML^{-1}T^{-1}]$
ν_{hnf}	Kinematic viscosity of hybrid nanofluid: Unit (m^2s^{-1}), Dimension $[L^2T^{-1}]$
u_o	Velocity of thin Needle: Unit (ms^{-1}), Dimension $[LT^{-1}]$
$\rho_{hnf,}$	Density of hybrid nanofluid: Unit (kgm^{-3}), Dimension $[ML^{-3}]$
$\rho_{f,}$	Density of base fluid: Unit $(kgm^{-3}),$Dimension$[ML^{-3}]$
k_{hnf}	Thermal conductivity of hybrid nanofluid: Unit $(Wm^{-1}.K^{-1})$, Dimension$[MLT^{-3}K^{-1}]$
k_f	Thermal conductivity of base fluid Unit $(Wm^{-1}.K^{-1})$, Dimension$[MLT^{-3}K^{-1}]$
$(C_P)_{hnf}$	Specific heat of hybrid nanofluid: Unit $(Jkg^{-1}.K^{-1})$, Dimension$[LT^{-2}K^{-1}]$
$(C_P)_f$	Specific heat of base fluid: Unit $(Jkg^{-1}.K^{-1})$, Dimension$[LT^{-2}K^{-1}]$
σ_{hnf}	Electrical conductivity of hybrid nanofluid: Unit (Sm^{-1}), Dimension$[M^{-1}L^{-3}T^3A]$
σ	Electrical conductivity Electrical conductivity: Unit (Sm^{-1}), Dimension$[M^{-1}L^{-3}T^3A]$
$R(x)$	Represents the shape of the axisymmetric body
x, r	Considered coordinates: Unit $(m),$Dimension$[L]$
T	Temperature of the fluid: Unit (K)Dimension$[K]$
T_o	Temperature of the surface of thin needle Unit $(K),$Dimension$[K]$
T_∞	Temperature of free stream region Unit (K), Dimension$[K]$
Γ	Time constant
φ	Nanoparticles shape parameter
u, v	Velocity components in x and y: directions: Unit; (m/s), Dimension$[LT^{-1}]$
B_o	Magnetic field strength: Unit (As^{-1})Dimension$[MI^{-1}T^{-2}]$
We	Williamson fluid parameter
C	Thin needle Thickness: Unit $(m),$ Dimension $[L]$
δ	Velocity ratio
U_o	Composite velocity: Unit ms^{-1}, Dimension $[LT^{-1}]$
M	Magnetic field parameter
u_∞	Free stream velocity: Unit (ms^{-1}), Dimension $[LT^{-1}]$
K	Porous medium parameter
α_{hnf}	Thermal diffusivity of hybrid nanofluid: Unit (m^2s^{-1}), Dimension$[L^2T^{-1}]$
α_f	Thermal diffusivity of base fluid: Unit (m^2s^{-1}), Dimension$[L^2T^{-1}]$
A, B	Non-uniform heat rise/fall parameter
η	Similarity variable
K_1	Porosity of the porous medium: Unit $(kg/m),$:, Dimension$[ML^{-1}]$
φ_{s1}	Volume fraction of solid nanoparticles (AA7075)
φ_{s2}	Volume fraction of solid nanoparticles AA7072
C_f	Skin friction coefficient
Nu_x	Nussle number
ψ	Stream function
Pr	Prandtl number
NFs	Newtonian Fluids
NNFs	Non-Newtonian Fluids
∞	Ambient conditions
o	Wall conditions

1. Introduction

In recent decades, nanotechnology has become the most important field that contributes effectively to improving the standard of living, reducing energy consumption, achieving economic efficiency, and improving product quality [1]. This notion is continuously being pursued as an effort to improve the well-being of society. A fluid that contains particles with nanometer dimensions is known as a nanofluid (NF). The NF is a colloidal suspension of the base liquid containing nanoparticles (NPs). NPs are utilized in the creation of nanofluids and can be comprised of various materials, including carbon-based materials, metals, and semiconductors [2]. The use of NF (nanofiltration) is crucial in the field of nanotechnology as it has a wide range of applications in various industries such as energy,

Fig. 1. Diagram of the practical uses of NF.

Table 1
Numerical and analytical methods used to solve hybrid NF flow.

Author(s)	Hybrid NPs	Numerical and analytical approach
Ref [19]	MoS_2–F e_3O_4/ethylene glycol	Galerkin method
Ref [20]	TiO_2–MWCNTs/pure water	Runge–Kutta method
Ref [21]	MoS_2-Go/Engine oil	Homotopy Analysis Method (HAM)
Ref [22]	Fe_2O_3 –Al_2O_3/water	Finite difference method
Ref. [23]	Al_2O_3–Cu/Ethylene glycol	Homotopy Analysis Method (HAM)
Ref [24]	CNT + Fe_3O_4/pure water	Homotopy Analysis Method (HAM)

electronics, the food industry, and pharmaceuticals [3]. NF exhibits superior thermal conductivity properties when compared to traditional liquids like alcohol, engine oil, paint, and kerosene. In order to improve the ability of a conventional liquid to transfer heat, tiny particles from an NF are mixed into a liquid base [4]. Therefore, the addition of metal particles in the nanometer range or metal oxide to a base fluid can improve its thermal conductivity. According to the findings of Eastman et al. [5], the addition of copper NPs at a concentration of 0.3% resulted in a significant improvement in thermal conductivity by 40% for ethylene-glycol fluid. Das et al. [6] discovered that adding aluminum oxide NPs in concentrations between 1 and 4% can increase the heat conductivity of water-based liquids by 10–25%. Rehan et al. [7] conducted an experimental study on using iron (III) oxide/hydroxide and aluminum oxide/-hydroxide NF in a parabolic solar energy concentrator trough. The study involved varying the concentration of the nanoparticles from 0.2 to 0.3 %. The results showed that using the nanofluid exhibited excellent performance, especially during winter, which could provide a reliable source of domestic energy supply using NF. Numerous studies have focused on the impact of additional thermofluid terms on increasing the thermal conductivity of NF, which can be found in Refs. [8,9]. However, experimental outcomes suggest that dispersing multiple kinds of NPs into the working fluid results in greater enhancements to the thermal conductivity of NF.

Researchers are showing a lot of interest in hybrid nanofluids (HNF) because they possess superior thermal characteristics [10]. These innovative fluids incorporate two distinct types of nanoparticles, resulting in enhanced heat transfer capabilities compared to both primary liquids and standard nanofluids [11]. As a result, they are widely used in machining and manufacturing processes, particularly in applications such as heat exchangers and refrigeration systems for energy storage [12]. Waini et al. [13] numerically investigated the permeable moving thin needle and steady flow of bifurcation using HNF (copper and alumina NPs) and compared it to pure water. Qureshi [14] investigated the entropy production and thermal energy distribution of an HNF that can be used for solar thermal energy in airplanes. According to the findings, the HNF with a mixture of cobalt ferrite and ethylene glycol has demonstrated an enhancement in thermal effectiveness between 3.8 % and 4.8 %, as compared to the Copper/Ethylene Glycol NF. Based on theoretical and experimental evidence [15,16], it has been shown that a mixture of two or more NPs can increase the thermal conductivity of a liquid compared to a single NF. This observation provides valuable insights into the potential for improving thermal transfer in many industrial uses. Fig. 1 shows various significant real-world applications of NF [17].

The investigation into the movement of fluids around a thin needle has become a topic of significant importance to researchers due to its significant applications in industrial fields such as medical and healthcare, hot wire anemometers, microelectronics, and geothermal power generation. Firstly, the analysis of the movement of fluids over a thin needle, was investigated by Lee [18], and then

several researchers [22–29] focused on this configuration by studying the effect of different governing parameters. Table 1 outlines various numerical and analytical approaches to estimating solutions for thin needle problems by utilizing hybrid NPs.

The principle of viscosity distinguishes fluids into two categories, which are Newtonian fluids (NFs) and non-Newtonian fluids (NNFs) [25]. Recently, NFs have gained the attention of researchers because of their diversified usage in industry. NNFs are substances that show variable levels of viscosity or resistance to flow under distinct levels of stress. Some common applications of NNF are toothpaste, cosmetics, blood, and soups. NNFs hold immense potential for addressing a wide range of challenges encountered in diverse industries, including petroleum engineering and medicine. NNFs have demonstrated their practicality in addressing real-world challenges, such as refining industrial procedures like oil extraction or boosting drug transportation systems [26]. To illustrate, the fluid utilized in oil wells to facilitate drilling is a non-Newtonian liquid that holds up drill cuttings, which in turn prevents them from settling at the bottom of the well. Similarly, blood acts as a non-Newtonian fluid with unique behaviors under varying conditions, requiring special considerations in medical treatments. Numerous rheological models have been established to illustrate the behavior of NNFs. The kind of model used depends on the specific rheological properties of the liquid. Several rheological models have been developed to describe the behavior of non-Newtonian fluids. The type of model used depends on the specific rheological properties of the fluid. Williamson fluid (WF), tangent hyperbolic and grade three fluids, and Maxwell fluid are some of the fluids used to characterize the results of NNF. The Williamson fluid rheological models have attracted a significant amount of focus among researchers in the field of NNF. The Williamson fluid is a type of fluid that becomes less viscous as the rate of shear stress increases. It is commonly used in various applications, such as the production of photographic films, the food industry, the flow of plasma, and drilling fluids. In 1929, Williamson studied the flow behavior of pseudoplastic materials and developed an equation to explain how these fluids flowed under different conditions. When HNF is created using this particular fluid as a base, the resulting nanofluid exhibits superior thermal and mechanical characteristics when compared to conventional fluids. Several scholars are actively engaged in investigating the behavior of pseudo-plastic fluids through a rheological Williamson model of HNF. The utilization of WF within HNF has the potential to boost their thermal and mechanical qualities while also revealing distinct flow behavior. Hussain et al. [27] employed a Williamson fluid model to study the influence of Cu-SA and GO-Cu/SA hybrid nanofluid radiative flow on a moving horizontal plate. Rashad et al. [28] utilized the RKF45 method via shooting to examine the Williamson fluid model of hybrid nanoparticles (Ag–TiO2/water) under convective boundary conditions. Some of the recently relevant published works are [29–32].

Magnetohydrodynamics (MHD) is the study of the dynamics of fluids that are influenced by electromagnetic forces, also known as magnetic liquid factors or hydromagnetic [33]. The area of study referred to as “magnetic hydrodynamics” is named after the word “magneto,” which implies attraction, “hydro,” which refers to water, and “dynamics,” which pertains to growth [34]. It explores the effects of magnetic fields on fluids like water [35]. MHD involves a combination of conditions that are based on both the Navier-Stokes equations for fluid mechanics and Maxwell’s electromagnetic equations [36]. It is important to consistently determine and apply these specific conditions in a logical and mathematical manner. MHD has a useful application in hybrid nanofluid flow, a technique that involves blending nanoparticles and base fluids for heat transfer purposes. In this method, the introduction of magnetic fields into the mixture allows researchers to regulate its flow behavior and enhance the transfer of heat. This technology holds promise in a variety of fields, including aerospace, electronics cooling, energy systems, and medical devices. For instance, Pasha et al. [37] determined the influences of the Yamada-Ota and Xue HNF on the MHD buoyancy-driven rotating cone with Smoluchowski temperature slip boundary conditions. Alshehri et al. [38] use the Cash-Karp numerical method to analyze the aluminum alloy and pure water nanofluid flow of two-dimensional electric field quality on a magnetohydrodynamic nonlinear uneven expanding sheet. Salawu et al. [39] took into consideration the Chebyshev collocation scheme to analyze the magnetized flow of Cu–Al_2O_3/$C_3H_8O_2$HNF on an elastic exponential temperature surface with electrochemical reactions.

The studyof the fluid flow through porous media, particularly regarding the implementation of thin needles, has gotten a lot of attention in the last two decades. An interesting area of investigation involves the performance of thin needles when they are incorporatedinto a porous medium. A porous medium is a substance described by its ability to allow liquids to flow through it due to the occurrence of small spaces. This phenomenon holds substantial potential for practical applications across numerous industries, such as thermal insulation, oil recovery, chemical catalysis, materials science, and so on. Over the past few years, several authors have conducted investigations on both the performance of the thin needles and fluid movement through porous medium. In regard to this, a numerical review of the nanofluid flow performance of a thin needle immersed in a porous medium was conducted by Akinshilo et al. [40], utilizing a non-Newtonian fluid model. Moreover, a numerical study was assessed by Bano et al. [41] to investigate the optically dense viscous incompressible fluid past a permeable moving thin needle. References [42,43] provide additional information pertaining to the fluid movement through a porous medium. Some relevant studies to the proposed problem are present in Refs. [44–53]. Ishak et al. [54] focused on the problem of fluid and heat transfer by moving thin needle in a parallel stream. Ashwinkumar et al. [55] presented the solutions of problem concentrating on the hybrid nanofluid Sakiadis flow due to thin needle. Ramesh et al. [56] gave the observation on Blasius and Sakiadis Williamson flow with convective boundary conditions.

This study examines the MHD fluid flow and heattransfer of a Williamson AA7075-AA7072/Methanol HNFflow over an incessantly moving thin needle embedded in a porous medium under the effect of internal heat generation. The main goals of this research are to investigate the influence of different control parameters like the Weissenberg number, porous medium parameter, and heat source on the thermal transport rate and flow characteristics. Also, to investigate the influence of porous medium on HNF flow and heat transfer over a moving thin needle. This research has identified the best design parameters that can be used to develop more effective systems for transferring heat and fluid flow. The findings of this study can be applied to various industries, including the food and agriculture sector, automotive, and power generation.

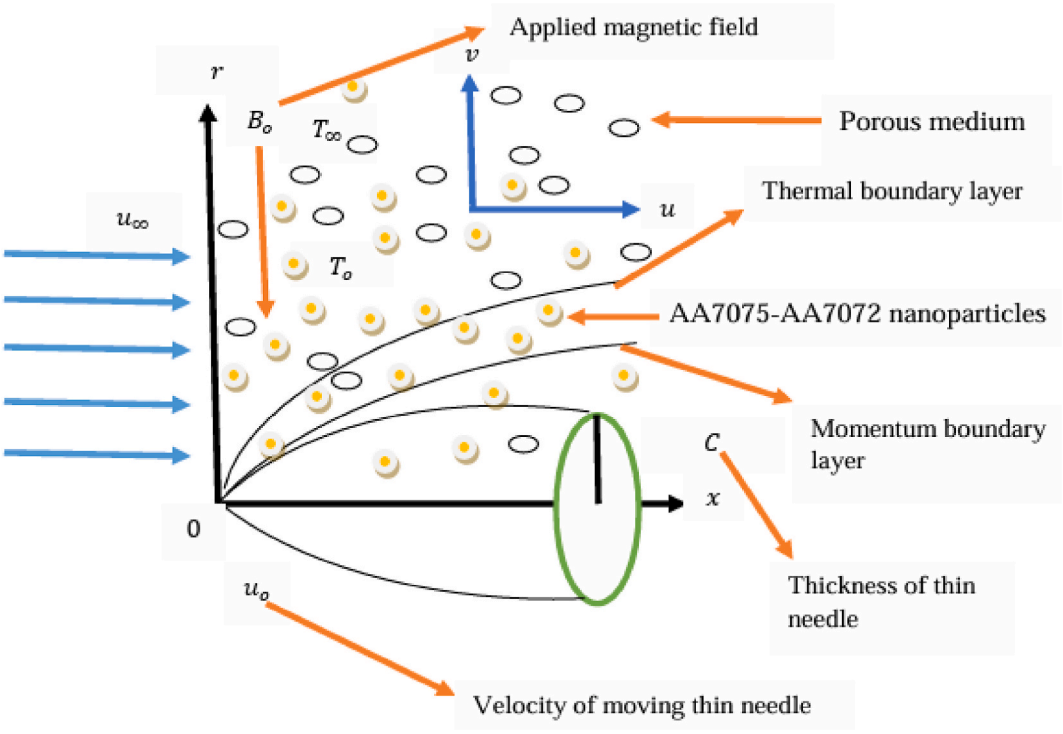

Fig. 2. Studied configuration.

2. Mathematical modeling

The following assumptions and characteristics are considered in the current model:

1. Two-dimensional boundary layer flow of electrically conducting Williamson Hybrid is assumed.
2. An incessantly thin moving needle is considered.
3. A uniform magnetic field having a magnitude B_o transverseto fluid flow is applied.
4. The non-uniform heat rises, and fall are considered in the current study.
5. The flow situation is being dealt in cylindrical coordinates (x, r) which signify axial and radial components, respectively.
6. The parabolic configured needle occupies thickness c whereas its width is presumed to be pretty less than the boundary layer formed around it and its movement in the flow is attributed to velocity u_o which could be along or antithesis of velocity of mainstream u_∞.
7. The presumption regarding temperature of the metallic needle T_o is and that of ambient fluid is T_∞ with assumption $(T_o > T_\infty)$.
8. The momentum boundary layer, and thermal boundary layer with flow scenario are presented in detail in Fig. 2

By following [54–56], the leading equations of boundary layer flow denoting the conservation law of mass, momentum, energy, and concentration are depicted as following:

$$\frac{\partial}{\partial x}(ru) + \frac{\partial}{\partial r}(rv) = 0, \tag{1}$$

$$\rho_{hnf}\left(u\frac{\partial u}{\partial x} + v\frac{\partial u}{\partial r}\right) = \mu_{hnf}\frac{1}{r}\frac{\partial}{\partial r}\left(r\frac{\partial u}{\partial r}\right) - \sigma_{hnf}B_o^2 u + \sqrt{2}\Gamma\mu_{hnf}\left(\frac{\partial u}{\partial r}\right)\frac{1}{r}\frac{\partial}{\partial r}\left(r\frac{\partial u}{\partial r}\right) - \frac{\frac{\mu_{hnf}}{\rho_{hnf}}}{K_1}u, \tag{2}$$

$$\left(\rho C_p\right)_{hnf}\left(u\frac{\partial T}{\partial x} + v\frac{\partial T}{\partial r}\right) = k_{hnf}\frac{1}{r}\frac{\partial}{\partial r}\left(r\frac{\partial T}{\partial r}\right) + q''', \tag{3}$$

Eqs. (1)–(4) are subjected to the following imperative boundary conditions.

$$\left.\begin{array}{c} u = u_o, v = 0, \theta(c) = 1, T = T_o, \text{at } r = R(x) \\ u \to u_\infty, T \to T_\infty \text{ as} r \to \infty \end{array}\right\}, \tag{4}$$

Table 2
Thermophysical properties [55].

Properties	$\rho(Kg/m)$	C_p $(JKg^{-1}K^{-1}$	k $(Wm^{-1}K^{-1})$	$\sigma(S/m)$
Methanol	792	2545	0.2035	0.5×10^{-6}
AA7075	2810	960	173	26.77×10^{6}
AA7072	2720	893	222	34.83×10^{6}

The axial and radial velocity components are represented by u and v, respectively. T is the temperature of the hybrid nanofluid, and $R(x)$ represents the shape of the axisymmetric body. The density, absolute viscosity coefficient, electrical conductivity, and thermal conductivity for hybrid nanofluid are respectively, denoted by ρ_{hnf}, μ_{hnf}, σ_{hnf} and k_{hnf}. Here, K_1 is permeability of the porous medium. Furthermore, Γ is named as time constant, C_p specifies the specific heat at constant pressure,and varying heat rise/fall in the energy equation is illustrated by $q''' = (k_f U_o/\nu_f x)[A(T_o - T_\infty)f' + B(T - T_\infty)]$.

3. Solutions methodology

This section illustrates the numerical procedure to solve Eqs. (1)–(3) along with the fixed boundary conditions (Eq. (4)). The subsequent subsections highlight the entire solution procedure through which partial differential equations will be transformed into ordinary differential equations, and then solved numerically by using numerical solver bvp4c.

3.1. Similarity variable formulation

The solution of coupled and non-linear partial differential equations is difficult; therefore, they are first transformed to ordinary differential equations by stream function formulation used by Ref. [55]. The similarity variables in form of stream function ψ are given below:

$$\left.\begin{aligned} \psi = \nu_f x f(\eta), u = r^{-1}\psi_r, v = -r^{-1}\psi_x, R(x) = \left(\frac{\nu_{fxC}}{U_o}\right)^{1/2} \\ \theta(\eta) = \frac{T - T_\infty}{T_o - T_\infty}, \eta = \frac{U_o r^2}{\nu_f x} \end{aligned}\right\}, \tag{5}$$

Here, η is similarity variable, and ν_f is kinematic viscosity of the fluid. The surface configuration (radius) of thin needle is related by $R(x)$ and $U_o = u_o + u_\infty$ signifies the composite velocity. In Table 2, the thermophysical properties of the fluid and nanoparticles are given.

By following [55], the expressions of the thermophysical properties of hybrid nanofluids areas follow:

$$\left.\begin{aligned} \frac{k_{hnf}}{k_f} = \frac{2(1-\varphi)k_f + (1+2\varphi_{1s})k_{1s} + (1+2\varphi_{2s})k_{2s}}{(2+\varphi)k_f + (1-\varphi_{1s})k_{1s} + (1-\varphi_{2s})k_{2s}} \\ \frac{(\rho C_p)_{hnf}}{(\rho C_p)_f} = (1-\varphi) + \frac{\varphi_{1s}(\rho C_p)_{1s} + \varphi_{2s}(\rho C_p)_{2s}}{(\rho C_p)_f} \\ \frac{\sigma_{hnf}}{\sigma_f} = 1 + \frac{3(\sigma_{1s}\varphi_{1s} - \varphi\sigma_f) + \varphi_{2s}\sigma_{2s}}{\sigma_{1s}(1-\varphi_{1s}) + \sigma_{2s}(1-\varphi_{2s}) + (2+\varphi)\sigma_f} \\ \frac{\rho_{hnf}}{\rho_f} = (1-\varphi) + \frac{\varphi_{1s}\rho_{1s} + \varphi_{2s}\rho_{2s}}{\rho_f} \\ \frac{\mu_{hnf}}{\mu_f} = \frac{1}{(1-\varphi)^{2.5}} \end{aligned}\right\}, \tag{6}$$

where φ_{1s} and φ_{2s} are volume fractions of nanoparticlesAA7075 and AA7072,respectively. After using Eq. (5) into Eqs. (1)–(4), then the transformed equations are given below:

$$\frac{2\mu_{hnf}}{\mu_f}(2W_e\eta f'' + 1)(\eta f''' + f'') + \frac{\rho_{hnf}}{\rho_f}ff'' - \frac{\sigma_{hnf}}{\sigma_f}Mf' - \frac{\mu_{hnf}}{\mu_f}/\frac{\rho_{hnf}}{\rho_f}Kf' = 0, \tag{7}$$

$$\theta'' + \left(\frac{1}{\eta} + \frac{k_f}{k_{hnf}}\frac{Pr}{2\eta}\frac{(\rho C_p)_{hnf}}{(\rho C_p)_f}f\right)\theta' + \frac{k_f}{k_{hnf}}\frac{}{4\eta}(Af' + B\theta) = 0, \tag{8}$$

Boundary conditions are:

$$\left.\begin{array}{c} f(C)=\dfrac{\delta C}{2}, f^{'}(C)=\dfrac{\delta}{2}, \theta(C)=1, \text{at } \eta=C \\ f^{'}(\eta)\rightarrow\dfrac{1-\delta}{2}, \theta(\eta)\rightarrow 0, \text{as} \eta\rightarrow\infty \end{array}\right\}, \tag{9}$$

Dimensionless parameters in dimensionless Eqs. (7)–(9) areporous medium parameter $K=\nu/K_1$, magnetic parameter $\left\{M=\frac{\sigma_f B_0^2 x}{2U_o\rho_f}\right\}$, Weissenberg number $\left\{W_e=\frac{2\sqrt{2}\Gamma U_o}{\nu r}\right\}$, velocity ratio $\left\{\delta=\frac{u_o}{U_o}\right\}$, Prandtl number $\left\{Pr=\frac{\nu_f}{\frac{(\mu C_p)_f}{k_f}}\right\}$, C is thickness of thin needle, $\delta=u_o/\,U_o$ is velocity ratio, and $U_o=u_o+u_\infty$ is composite velocity, A and B non-uniform heat rise and fall parmaters.

By following [55], the physical quantities of engineering interestwhich are the skin friction coefficient C_f, and local Nusselt number Nu_x are defined as follow:

$$C_f=\frac{\mu_{hnf}}{\rho_f U_0^2}\left(\frac{\partial u}{\partial r}\right)_{r=c}, Nu_x=-\frac{xk_{hnf}}{k_f(T_o-T_\infty)}\left(\frac{\partial T}{\partial r}\right)_{r=c} \tag{10}$$

By following [55] and performing some algebra utilizing (6), we lastly achieve the given dimensionless structure.

$$\left.\begin{array}{c} \dfrac{Re_x^{1/2}C_f}{4c^{1/2}}=\dfrac{\mu_{hnf}}{\mu_f}f^{''}(c) \\ \dfrac{Re_x^{-1/2}Nu_x}{2c^{1/2}}=-\dfrac{k_{hnf}}{k_f}\theta^{'}(c) \end{array}\right\} \tag{11}$$

where $Re_x=\frac{U_o x}{\nu_f}$ stands for local Reynolds number.

3.2. Solution technique

Eqs. 7–10 and Eq. (11) are solved usingbvp4csolver. This solver is based on the collocation formula. Equations (7) and (8) with boundary conditions specified in Equation (9) are converted first into first order ordinary differential equations, which are then fed into MATLAB's bvp4c numerical algorithm to provide numerical results. By following [55], the approach to the solution is provided below:

$$\Gamma(1)=f, \Gamma(2)=f^{'}, \Gamma(3)=f^{''}, \Gamma(4)=\theta, \Gamma(5)=\theta^{'}, \tag{12}$$

$$\Gamma\Gamma 1=\frac{\mu_f}{2*\mu_{hnf}(2*W_e*\eta*\Gamma(3)+1)}+\frac{\Gamma(3)}{2}+\frac{\mu_f*\frac{\rho_{hnf}}{\rho_f}*\Gamma(1)*\Gamma(3)}{2*\mu_{hnf}*(2*W_e*\eta*\Gamma(3)+1)}-\frac{\frac{\mu_f}{\mu_{hnf}}*\frac{\sigma_{hnf}}{\sigma_f}*M*\Gamma(2)}{(2*W_e*\eta*\Gamma(3)+1)}-\frac{\frac{\mu_f}{\mu_{hnf}}}{\frac{\rho_{hnf}}{\rho_f}}*K*\frac{f^{'}}{(2*W_e*\eta*\Gamma(3)+1)}, \tag{13}$$

$$\Gamma\Gamma 2=\left(\frac{1}{\eta}+\frac{k_f*Pr*}{k_{hnf}*2*\eta}\frac{(\rho C_p)_{hnf}}{(\rho C_p)_f}*\Gamma(1)\right)*\Gamma(5)+\frac{k_f}{k_{hnf}4\eta}(A^*\Gamma(2)+B^*\Gamma(4))=. \tag{14}$$

Boundary conditions

$$\left.\begin{array}{c} \Gamma(1)=\dfrac{\delta C}{2}, \Gamma(2)=\dfrac{\delta}{2}, \Gamma(4)=1, \text{at } \eta=C \\ \Gamma(2)\rightarrow\dfrac{1-\delta}{2}, \Gamma(4)\rightarrow 0, \text{as } \eta\rightarrow\infty \end{array}\right\}. \tag{15}$$

4. Results and discussion

The graphical and tabular results for the unknown variables are presented in this section, along with physical interpretations of the effects of the governing parameters. The parameters under consideration in the current study are Porous medium parameter (K), Weissenberg number (We), velocity ratio(δ), Prandtl number (Pr), and needle thickness parameter C, magnetic number(M), nanoparticles shapes parameter (φ), and irregular heat rise/fall parameters A, and B. Graphs and tables arepresented for various values of volume fractions of nanoparticles (φ_1, φ_2), needle thickness parameter C, nanoparticles shapes parameter (φ),velocity ratio(δ), Weissenberg number (We), and Prandtl number (Pr), magnetic number(M), and irregular heat rise/fall parameters A, and B. The graphs are plotted for velocity theprofile and temperature distribution and tables are presented for Skin friction coefficient and Nusselt number.

Fig. 3 is revealing the effect of theporous medium parameter K on the velocity the velocity profile. TheVariations of $f^{'}$ indicatethat as K is increased, thevelocity decreases gradually. Here, it can be noted that thevelocity valuesrelative toAA7075/Methanol nanofluid

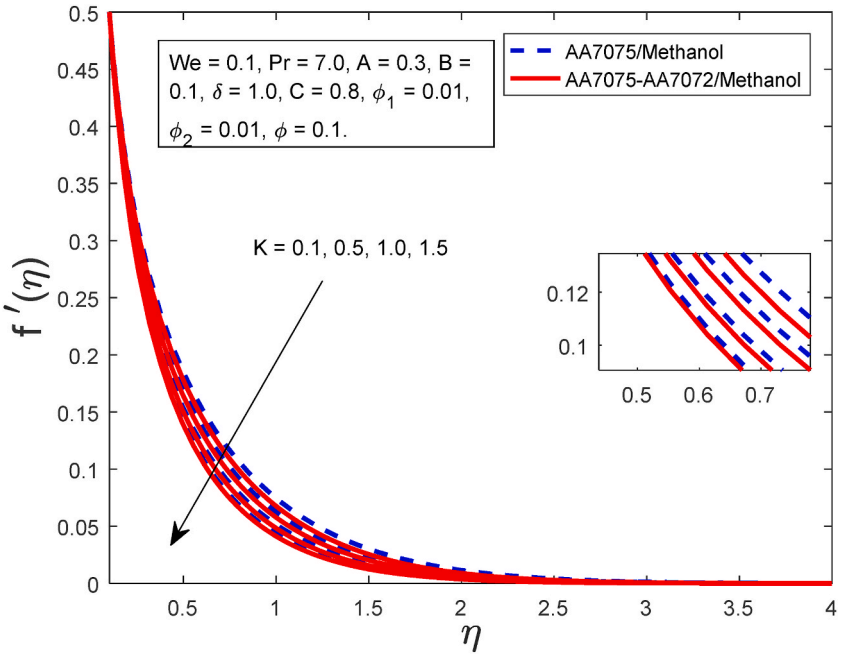

Fig. 3. Velocity profiles for various K values.

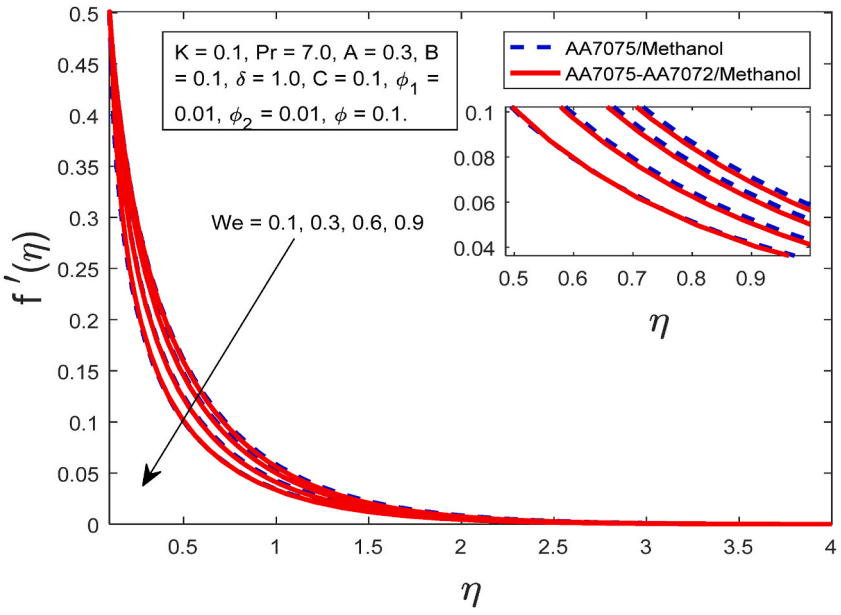

Fig. 4. Velocity profiles for various We values.

are higher than those of AA7075- AA7072/Methanol hybrid nanofluid. Physically, it is due to the increase of the viscous forces, and to the reduction of the pores size causing the deceleration in the fluid velocity. Which is in concordance with the definition ofthe porosity parameter. The graphical variations of f' for distinct values of Weissenberg number (We), are illustrated in Fig. 4. It is worthy to note that velocity declines for both AA7075/Methanol nanofluid and AA7075- AA7072/Methanol hybrid nanofluid, but higher magnitudes for AA7075/Methanolare seen as We is intensified. This is due to the fact that higher nanoparticles fraction causes the declination in flow velocity. Figs. 5–6 are sketched to show the behaviors of f' and θ for various values of magnetic field number. Graphs are depicting thatwhen M is risen f' goes down and θ goes up for bothAA7075/Methanol nanofluid and AA7075- AA7072/Methanol hybrid nanofluid. As per physical point of view by increasing M a resistive force called Lorentz force is producedin the opposite direction of the

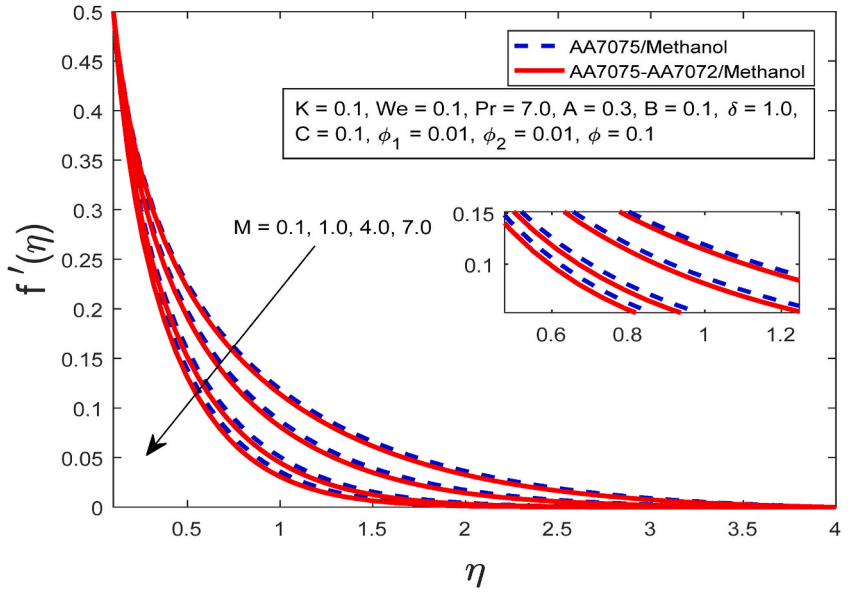

Fig. 5. Velocity profiles for various M values.

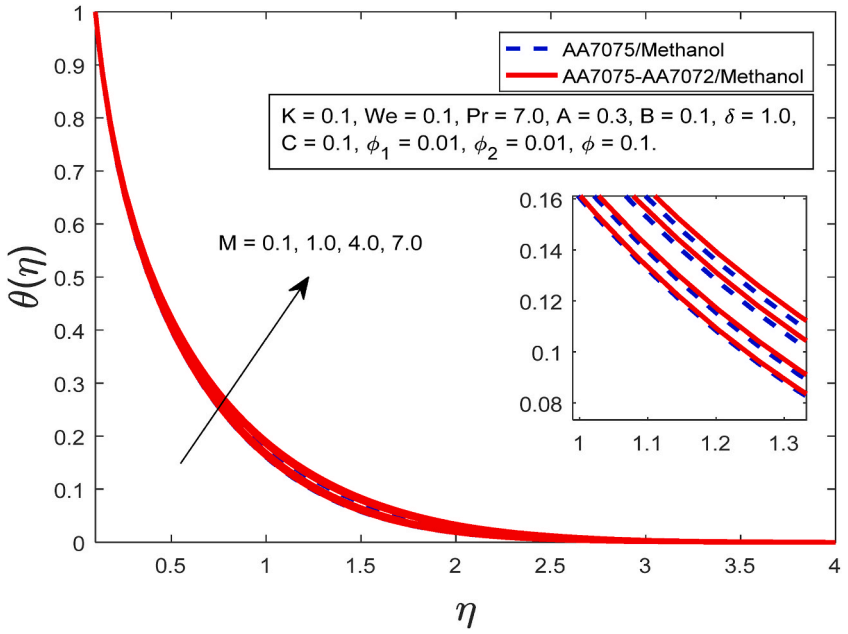

Fig. 6. Temperature profiles for various M values.

flow, leading to a considerable reduction of the fluid velocity and an augmentation of the temperature. Figs. 7–8 present the temperature profiles for various values of A and B respectively. It is worthy to note that for both non-uniform heat-rise and fall parameters, the temperature of the fluid gets stronger. Physically it endorses the purpose of consideration of heat rise and fall. Variations in $f^{'}$ and θ for various values of C are illustrated in Figs. 9 and 10 respectively. For both profiles, a reduction is seen against increasing thevalues of C. Figs. 11 and 12 are plotted to show the effect of varying the volume fractions φ_1 *and* φ_2 on the velocity and temperature profiles. It is noticed that, asthevolume fractions of both nanoparticles φ_1, φ_2 are augmented then $,f^{'}$ and θ are increasing rapidly. This is due to the enhanced thermophysical propertiescaused by the addition of nanoparticles.

In Table 3 the presented results for skin friction $f^{''}(c)$ are compared withthepreviouslypublished findingsof Ishak et al. [54] for different values of C. From thecomparison it has been concluded that there is strong agreement between the results that ensures the validation and accuracy of the current model and method of solution. Table 4 illustrates the results for skin friction coefficient and

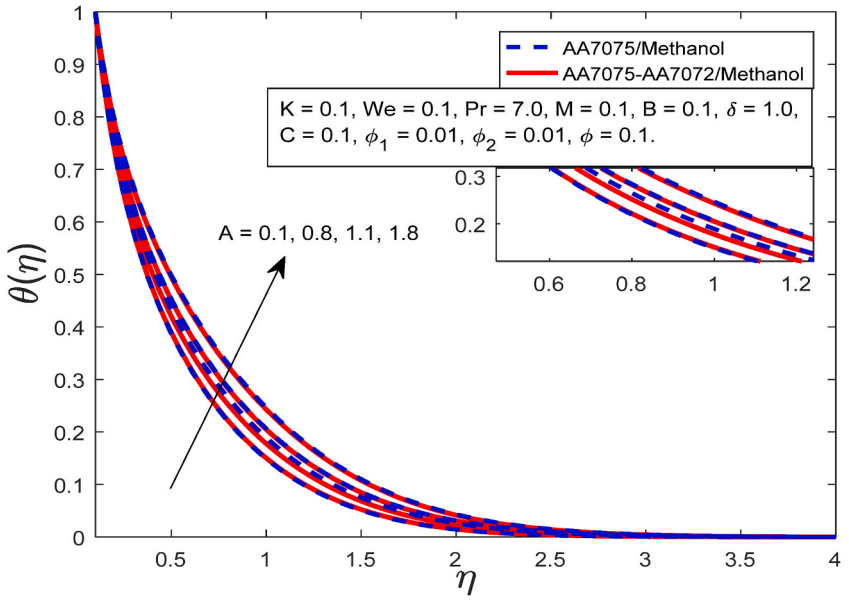

Fig. 7. Temperature profiles for various A values.

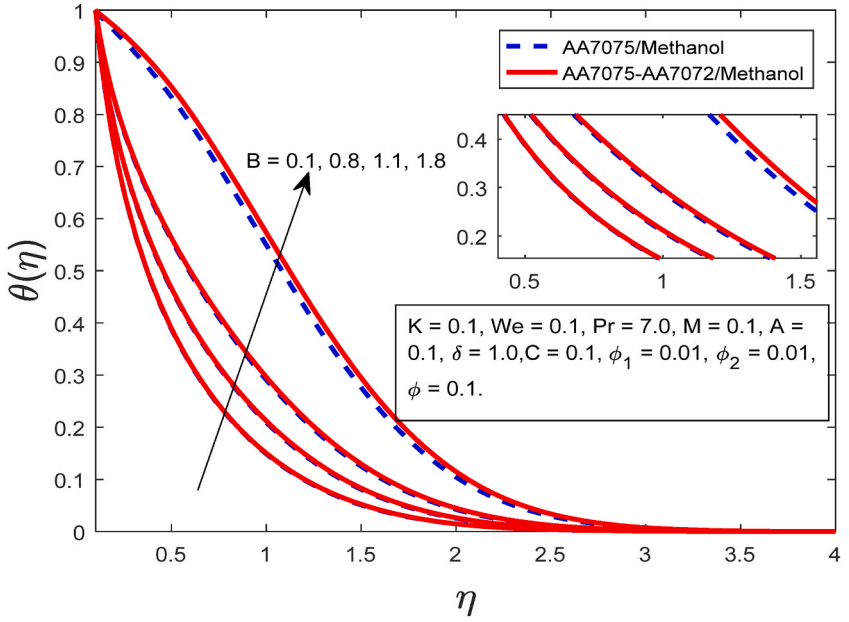

Fig. 8. Temperature profiles for various B values.

Nusselt number for distinct values of Weissenberg number (We), when the rest of parameters are kept constant. The results are indicating that $Re^{1/2}C_f$ is increasing and $Re^{-1/2}Nu$ are decreasingas We is raised. Table 5 is presented to illustrate the effect of the porous medium parameter on the skin friction coefficient and Nusselt number. When K is increased $Re^{1/2}C_f$ is risen and $Re^{-1/2}Nu$ declined accordingly.

5. Conclusion

The current investigation is based on the study of Williamson AA7075-AA7072/Methanol hybrid nanofluid flow over incessantly moving thin needle embedded in a porous medium in the presence of non-uniform heat rise/fall and magnetic field. The results in graphs and tables are shown in this study and the main findings are summarized as follow:

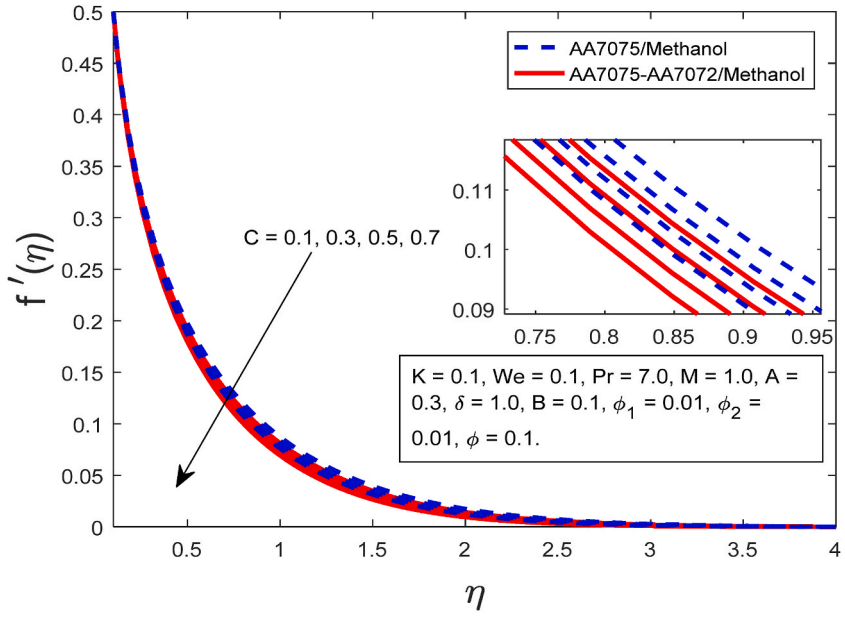

Fig. 9. Velocity profiles for various *C* values.

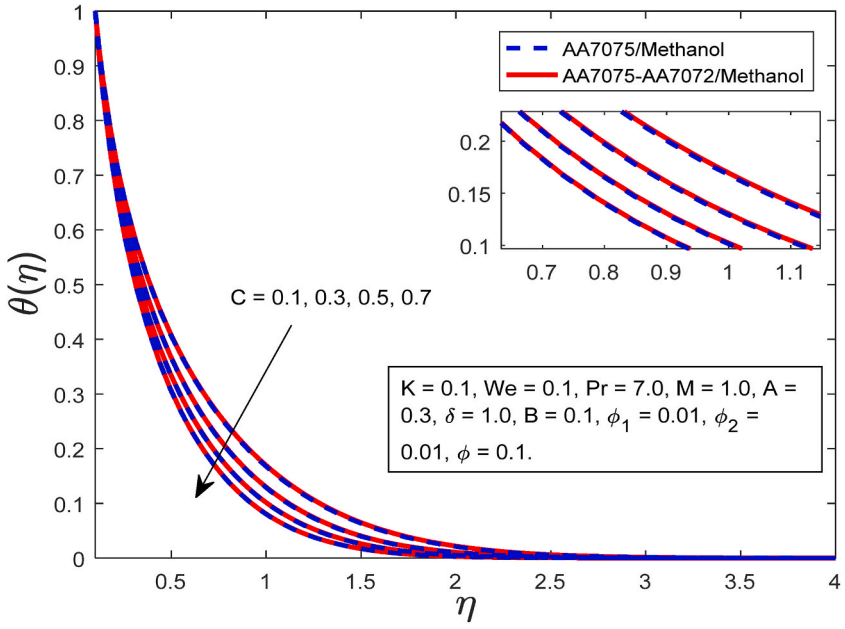

Fig. 10. Temperature profiles for various *C* values.

- It is worthy to note that the velocity declines for both AA7075/Methanol nanofluid and AA7075- AA7072/Methanol hybrid nanofluid, but higher magnitudes for AA7075/Methanol is seen as Williamson fluid parameter is intensified.
- It is concluded from the velocityprofiles that as the porous medium parameter is increased, the velocity decreases gradually.
- It is noticed that as volume fractions of both nanoparticles are augmented then velocity and temperature of fluid are increasing rapidly.
- Graphs are depicting that when *M* is risen, velocity goes down and temperature goes up for bothAA7075/Methanol nanofluid and AA7075- AA7072/Methanol hybrid nanofluid.
- Comparison of current and published results is given for validation of proposed study.

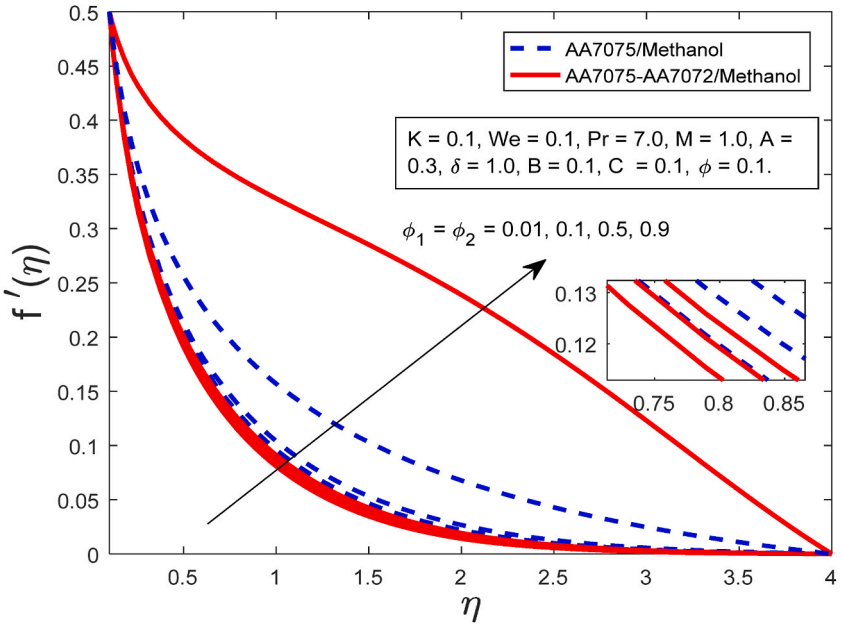

Fig. 11. Velocity profiles for various φ_1 *and* φ_2 values.

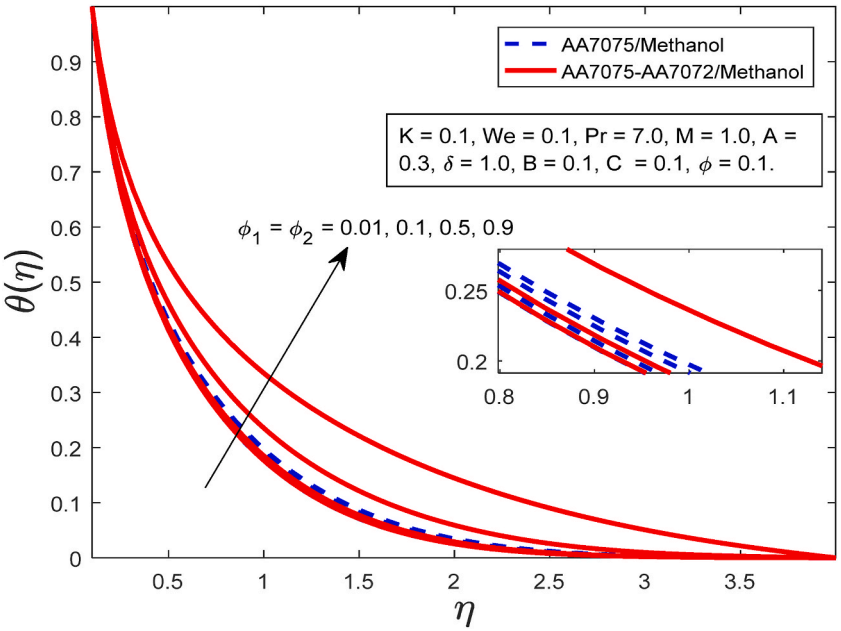

Fig. 12. Temperature profiles for various φ_1 *and* φ_2 values.

Table 3
Comparison of $f''(0)$, with the results of Ishak et al. [54].

C	Ishak et al. [54]	Present
0.1	1.2888	1.2887
0.01	8.4924	8.4913
0.001	62.1637	62.1626

Table 4
Values of $Re^{1/2}C_f and Re^{-1/2}Nu$ for $Pr = 1.0, M = 0.1, A = 0.3, B = 0.1, \delta = 1.0, C = 0.1, \varphi_1 = \varphi_2 = 0.01, K = 0.1$ and various values of We.

We	$Re^{1/2}C_f$	$Re^{-1/2}Nu$
0.1	−1.472040092258348	2.938462673540185
0.3	−1.655696759471036	2.928808557391347
0.5	−1.908561541970002	2.918163659374573
0.7	−2.291843883524330	2.906402813419327

Table 5
Values of $Re^{1/2}C_f and Re^{-1/2}Nu for M = 1.0, We = 0.1, A = 0.3, B = 0.1, \delta = 1.0, C = 0.1, \varphi_1 = \varphi_2 = 0.01, Pr = 7.0$ and variousvalues of K.

K	$Re^{1/2}C_f$	$Re^{-1/2}Nu$
0.1	−1.472040092258348	2.938462673540185
0.3	−1.548791659714867	2.929465643930223
0.5	−1.615545627255709	2.921788950032734
0.7	−1.674594140180696	2.915139356878290

Data availability statement

Data sharing is not applicable to this article as no new data were created or analyzed in this study.

CRediT authorship contribution statement

Amir Abbas: Writing - review & editing, Writing - original draft, Software, Data curation, Conceptualization. **Abid Hussanan:** Validation, Software, Formal analysis, Data curation. **Adebowale Martins Obalalu:** Writing - review & editing, Visualization, Software, Formal analysis. **Karim Kriaa:** Supervision, Resources, Project administration. **Chemseddine Maatki:** Supervision, Resources, Project administration, Funding acquisition. **Bilel Hadrich:** Visualization, Validation, Supervision, Software, Resources. **Muhammad Aslam:** Visualization, Validation, Software, Methodology, Investigation. **Lioua Kolsi:** Visualization, Supervision, Project administration, Methodology, Investigation.

Declaration of competing interest

The authors declare that they have no known competing financial interests or personal relationships that could have appeared to influence the work reported in this paper.

Acknowledgements

This work was supported and funded by the Deanship of Scientific Research at Imam Mohammad Ibn Saud Islamic University (IMSIU) (grant number IMSIU-RG23099).

References

[1] Y.M. Chu, S. Bilal, M.R. Hajizadeh, Hybrid Ferrofluid along with MWCNT for Augmentation of Thermal Behavior of Fluid during Natural Convection in a Cavity, 2020.
[2] D. Gamachu, W. Ibrahim, Entropy production on couple-stress hybrid nanofluid flow in a rocket engine nozzle with non-Fourier's and non-Fick's law, Ain Shams Eng. J. (2022), 101818.
[3] W. Ibrahim, Magnetohydrodynamics (MHD) flow of a tangent hyperbolic fluid with nanoparticles past a stretching sheet with second order slip and convective boundary condition, Results in physics 7 (2017) 3723–3731.
[4] S. Salawu, A. Obalalu, E. Fatunmbi, R. Oderinu, Thermal Prandtl-Eyring hybridized MoS2-SiO2/C3H8O2 and SiO2-C3H8O2 nanofluids for effective solar energy absorber and entropy optimization: a solar water pump implementation, J. Mol. Liq. 361 (2022), 119608.
[5] J.A. Eastman, S. Choi, S. Li, W. Yu, L. Thompson, Anomalously increased effective thermal conductivities of ethylene glycol-based nanofluids containing copper nanoparticles, Appl. Phys. Lett. 78 (6) (2001) 718–720.
[6] S.K. Das, N. Putra, P. Thiesen, W. Roetzel, Temperature dependence of thermal conductivity enhancement for nanofluids, J. Heat Transfer. 125 (4) (2003) 567–574.
[7] M.A. Rehan, M. Ali, N.A. Sheikh, M.S. Khalil, G.Q. Chaudhary, T. Ur Rashid, M. Shehryar, Experimental performance analysis of low concentration ratio solar parabolic trough collectors with nanofluids in winter conditions, Renew. Energy 118 (2018) 742–751.
[8] S. Salawu, A. Obalalu, E. Fatunmbi, M. Shamshuddin, Elastic deformation of thermal radiative and convective hybrid SWCNT-Ag and MWCNT-MoS4 magneto-nanofluids flow in a cylinder, Results in Materials (2023), 100380.
[9] S. Salawu, A. Obalalu, M. Shamshuddin, Nonlinear solar thermal radiation efficiency and energy optimization for magnetized hybrid Prandtl–eyring nanoliquid in aircraft, Arabian J. Sci. Eng. (2022) 1–12.
[10] E.H. Aly, I. Pop, MHD flow and heat transfer near stagnation point over a stretching/shrinking surface with partial slip and viscous dissipation: hybrid nanofluid versus nanofluid, Powder Technol. 367 (2020) 192–205.

[11] S. Bellout, R. Bessaïh, Mixed convection and entropy production of a hybrid nanofluid in a porous cylindrical enclosure with rotating top wall, Heat Transfer 51 (4) (2022) 3540–3561.
[12] A. Obalalu, H. Ahmad, S. Salawu, O. Olayemi, C. Odetunde, A. Ajala, A. Abdulraheem, Improvement of mechanical energy using thermal efficiency of hybrid nanofluid on solar aircraft wings: an application of renewable, sustainable energy. Waves in Random Complex Media, 2023, pp. 1–30.
[13] I. Waini, A. Ishak, I. Pop, Hybrid nanofluid flow past a permeable moving thin needle, Mathematics 8 (4) (2020) 612.
[14] M.A. Qureshi, Thermal capability and entropy optimization for Prandtl-Eyring hybrid nanofluid flow in solar aircraft implementation: thermal capability for Prandtl-Eyring hybrid nanofluid flow in solar aircraft, Alex. Eng. J. 61 (7) (2022) 5295–5307.
[15] A. Obalalu, S. Salawu, M.A. Memon, O. Olayemi, M.R. Ali, R. Sadat, C. Odetunde, O. Ajala, A. Akindele, Computational study of Cattaneo–Christov heat flux on cylindrical surfaces using CNT hybrid nanofluids: a solar-powered ship implementation, Case Stud. Therm. Eng. 45 (2023), 102959.
[16] Z. Xie, J. Jiao, K. Yang, Theoretical and experimental study on the fluid-structure-acoustic coupling dynamics of a new water lubricated bearing, Tribol. Int. 177 (2023), 107982.
[17] M. Abdul Basit, M. Imran, S.A. Khan, A. Alhushaybari, R. Sadat, M.R. Ali, Partial differential equations modeling of bio-convective sutterby nanofluid flow through paraboloid surface, Sci. Rep. 13 (2023) 1 6152.
[18] L.L. Lee, Boundary layer over a thin needle, Phys. Fluid. 10 (1967) 4 820–822.
[19] Z. Abbas, A.U. Rehman, S. Khaliq, M.Y. Rafiq, Flow dynamics of MHD hybrid nanofluid past a moving thin needle with a temporal stability test: a Galerkin method approach, Numer. Heat Tran., Part B: Fundamentals. (2023) 1–19.
[20] P. Prashar, O. Ojjela, P.K. Kambhatla, Impact of needle size and distinct flow conditions on thermal performance of TiO2–MWCNTs hybrid nanofluid flow past thin needle using Casson fluid model, ZAMM-Journal of Applied Mathematics. Mechanics/Zeitschrift für Angewandte Mathematik und Mechanik. (2023), e202100456.
[21] M. Ramzan, U. Shamshad, S. Rehman, M.S. Junaid, A. Saeed, P. Kumam, Analytical simulation of Hall current and Cattaneo–Christov heat flux in cross-hybrid nanofluid with autocatalytic chemical reaction: an engineering application of engine oil, Arabian J. Sci. Eng. 48 (2023) 3 3797–3817.
[22] S. Dinarvand, S.M. Mousavi, M. Yousefi, M. Nademi Rostami, MHD flow of MgO-Ag/water hybrid nanofluid past a moving slim needle considering dual solutions: an applicable model for hot-wire anemometer analysis, Int. J. Numer. Methods Heat Fluid Flow 32 (2022) 2 488–510.
[23] V.S. Reddy, J. Kandasamy, S. Sivanandam, Impacts of casson model on hybrid nanofluid flow over a moving thin needle with dufour and soret and thermal radiation effects, Math. Comput. Appl. 28 (2022) 1 2.
[24] T. Gul, M. Bilal, A. Saeed, W. Alghamdi, S. Mukhtar, H. Alrabaiah, E. Bonyah, Viscous dissipated hybrid nanoliquid flow with Darcy–Forchheimer and forced convection over a moving thin needle, AIP Adv. 10 (2020) 10.
[25] A.M. Obalalu, L.L. Adebayo, I. Colak, A.O. Ajala, F.A. Wahaab, Entropy generation minimization on electromagnetohydrodynamic radiative Casson nanofluid flow over a melting Riga plate, Heat Transfer (2022).
[26] K. Beazley, Non-Newtonian technology in the China clay industry, Chem. Eng. Sci. (1971) 16–19.
[27] S.M. Hussain, Dynamics of radiative Williamson hybrid nanofluid with entropy generation: significance in solar aircraft, Sci. Rep. 12 (2022) 1 8916.
[28] A.M. Rashad, M.A. Nafe, D.A. Eisa, Heat variation on MHD Williamson hybrid nanofluid flow with convective boundary condition and Ohmic heating in a porous material, Sci. Rep. 13 (2023) 1 6071.
[29] K. Loganathan, S. Rajan, An entropy approach of Williamson nanofluid flow with Joule heating and zero nanoparticle mass flux, Journal of Thermal Analysis Calorimetry 141 (2020) 6 2599–2612.
[30] A. Hamid, M. Khan, M. Alghamdi, Numerical simulation for transient flow of Williamson fluid with multiple slip model in the presence of chemically reacting species, Int. J. Numer. Methods Heat Fluid Flow 29 (11) (2019) 4445–4461.
[31] A. Hamid, A. Hafeez, M. Khan, A.S. Alshomrani, M. Alghamdi, Heat transport features of magnetic water–graphene oxide nanofluid flow with thermal radiation: stability Test, Eur. J. Mech. B Fluid 76 (2019) 434–441.
[32] A. Hamid, M. Alghamdi, M. Khan, A.S. Alshomrani, An investigation of thermal and solutal stratification effects on mixed convection flow and heat transfer of Williamson nanofluid, J. Mol. Liq. 284 (2019) 307–315.
[33] N.A. Aminuddin, N.A.A.M. Nasir, W. Jamshed, A. Ishak, I. Pop, M.R. Eid, Impact of thermal radiation on MHD GO-Fe2O4/EG flow and heat transfer over a moving surface, Symmetry 15 (3) (2023) 584.
[34] A. Dawar, Z. Shah, S. Islam, W. Deebani, M. Shutaywi, MHD stagnation point flow of a water-based copper nanofluid past a flat plate with solar radiation effect, Journal of Petroleum Science Engineering 220 (2023), 111148.
[35] F. Shahzad, W. Jamshed, T. Sajid, K. Nisar, M. Eid, Heat transfer simulation for 3D MHD rotating hybrid nanofluid flow between parallel plates in parabolic trough solar collector: a numerical study, J. Eng. Thermophys. 30 (4) (2021) 704–726.
[36] B. Kumbhakar, S. Nandi, Unsteady MHD radiative-dissipative flow of Cu-Al2O3/H2O hybrid nanofluid past a stretching sheet with slip and convective conditions: a regression analysis, Math. Comput. Simulat. 194 (2022) 563–587.
[37] A.A. Pasha, M.M. Rahman, W. Jamshed, K.A. Juhany, S.N. Pillai, Buoyancy driven flow and slippage constraints influences on Casson hybridity nanofluid of Yamada-Ota and Xue type via rotating cone, Ain Shams Eng. J. 14 (4) (2023) 101934.
[38] M.H. Alshehri, F.Z. Duraihem, R. Kandasamy, Impacts of electric field quality on MHD Carreau AA7075–water nanofluid flow, J. Taibah Univ. Sci. 14 (2020) 1 1402–1415.
[39] S. Salawu, A. Obalalu, S. Okoya, Thermal convection and solar radiation of electromagnetic actuator Cu–Al2O3/C3H8O2 and Cu–C3H8O2 hybrid nanofluids for solar collector optimization, Mater. Today Commun. 33 (2022), 104763.
[40] A. Akinshilo, F. Mabood, A. Ilegbusi, Heat generation and nonlinear radiation effects on MHD Casson nanofluids over a thin needle embedded in porous medium, Int. Commun. Heat Mass Tran. 127 (2021), 105547.
[41] N. Bano, B. Singh, An integral treatment for coupled heat and mass transfer by natural convection from a radiating vertical thin needle in a porous medium, Int. Commun. Heat Mass Tran. 84 (2017) 41–48.
[42] T. Nazar, M. Bhatti, E.E. Michaelides, Hybrid (Au-TiO2) nanofluid flow over a thin needle with magnetic field and thermal radiation: dual solutions and stability analysis, Microfluid. Nanofluidics 26 (2022) 1 2.
[43] S.K. Soid, A. Ishak, I. Pop, Boundary layer flow past a continuously moving thin needle in a nanofluid, Appl. Therm. Eng. 114 (2017) 58–64.
[44] M.B. Jeelani, A. Abbas, Al2O3-Cu\Ethylene glycol-based magnetohydrodynamic non-Newtonian Maxwell hybrid nanofluid flow with suction effects in a porous space: energy saving by solar radiation, Symmetry 15 (9) (2023) 1794.
[45] Thermal performance of Oldroyd-B hybrid nanofluid in solar energy-based water pumping systems and entropy generation minimization, Case Stud. Therm. Eng. 51 (2023), 103476.
[46] M.B. Jeelani, A. Abbas, Thermal efficiency of spherical nanoparticles Al2O3-Cu dispersion in ethylene glycol via the MHD non-Newtonian Maxwell fluid model past the stretching inclined sheet with suction effects in a porous space, Processes 11 (10) (2023) 2842.
[47] Significance of thermal density and viscous dissipation on heat and mass transfer of chemically reactive nanofluid flow along stretching sheet under magnetic field, Resulst in Engineering 20 (2023), 101413.
[48] Implication of electromagnetohydrodynamic and heat transfer analysis in nanomaterial flow over a stretched surface: applications in solar energy, Case Stud. Therm. Eng. 49 (2023), 103381.
[49] A. Abbas, M. Ashraf, H. Ahmad, K. Ghachem, Z. Ullah, A. Hussanan, L. Kolsi, Computational analysis of Darcy-Forchheimer relation, reduced gravity, and external applied magnetic field influence on radiative fluid flow and heat transfer past a sphere: finite difference method, Heliyon 9 (5) (2023), e15696.
[50] A. Abbas, I.E. Sarris, M. Ashraf, K. Ghachem, N. Hnaien, B.M. Alshammari, The effects of reduced gravity and radiative heat transfer on the magnetohydrodynamic flow past a non-rotating stationary sphere surrounded by a porous medium, Symmetry 15 (4) (2023) 806.
[51] A. Abbas, M. Ashraf, I.E. Sarris, K. Ghachem, T. Labidi, L. Kolsi, H. Ahmad, Numerical simulation of the effects of reduced gravity, radiation and magnetic field on heat transfer past a solid sphere using finite difference method, Symmetry 15 (3) (2023) 772.

[52] M. Ashraf, A. Khan, A. Abbas, A. Hussanan, K. Ghachem, C. Maatki, L. Kolsi, Finite difference method to evaluate the characteristics of optically dense gray nanofluid heat transfer around the surface of a sphere and in the plume region, Mathematics 11 (4) (2023) 908.
[53] A. Abbas, A. Noreen, M.A. Ali, M. Ashraf, E. Alzahrani, R. Marzouki, M. Goodarzi, Solar radiation over a roof in the presence of temperature-dependent thermal conductivity of a Casson flow for energy saving in buildings, Sustain. Energy Technol. Assessments 53 (2022), 102606.
[54] A. Ishak, R. Nazar, I. Pop, Boundary layer flow over a continuously moving thin needle in a parallel free stream, Chin. Phys. Lett. 24 (10) (2007) 2895.
[55] G.P. Ashwinkumar, Computational analysis on MHD Sakiadis flow of hybrid nanoliquid past an incessantly moving thin needle, Int. J. Model. Simulat. (2023) 1–12.
[56] G.K. Ramesh, B.J. Gireesha, R.S.R. Gorla, Study on Sakiadis and Blasius flows of Williamson fluid with convective boundary condition, Nonlinear Eng. 4 (4) (2015) 215–221.